Engineering Science and Technology, an International Journal 57 (2024) 101823

Contents lists available at ScienceDirect

Engineering Science and Technology, an International Journal

journal homepage: www.elsevier.com/locate/jestch

Real-time techno-economical operation of preserving microgrids via optimal NLMPC considering uncertainties

Elaheh Yaghoubi [a,*], Elnaz Yaghoubi [a], Ziyodulla Yusupov [a], Javad Rahebi [b]

[a] Department of Electrical and Electronics Engineering, Karabuk University, Karabuk, Turkey
[b] Department of Software Engineering, Istanbul Topkapi University, Istanbul, Turkey

ARTICLE INFO

Keywords:
Non-linear model predictive control
Techno-economical control
Real-time
Continuous power flow
Network preserving model

ABSTRACT

In the modern era, managing optimal real-time control of microgrids during the operation phase has been a significant challenge, requiring careful consideration of both technical and economic factors. This paper introduces a framework for the real-time control of islanded microgrids using a preserving network. This structure incorporates various distributed generation sources, including rotating and non-rotating resources, along with energy storage systems. The optimization function within model predictive control (MPC) manages essential network parameters, such as frequency and voltage, while addressing real-time economic and technical objectives. To enhance precision and account for uncertainties in generation and consumption parameters, the integration of continuous power flow and the preserving network model is employed. This approach aims to create a model that closely mirrors real-world conditions, ensuring a more accurate representation of microgrid dynamics. The proposed structure demonstrates significant improvements in both technical and economic performance compared to Standard MPC and Adaptive MPC, highlighting its potential for more efficient islanded microgrid management. The proposed framework achieves notable reductions in total voltage deviation of 85.87% and 87.62% compared to Standard MPC and Adaptive MPC, respectively. Additionally, it delivers impressive enhancements in frequency deviation of 99.46% and 96.62% compared to Standard MPC and Adaptive MPC, respectively. Economically, the proposed framework significantly outperforms both, reducing costs by 39.29% compared to Standard MPC and by 28.12% compared to Adaptive MPC.

1. Introduction

1.1. Importance and motivations

Microgrids, characterized by localized energy systems with distributed generation sources and controllable loads, have emerged as a crucial solution for enhancing grid resilience and advancing sustainability [1,2]. As the demand for efficient and reliable energy solutions continues to rise, the optimization of microgrid control becomes imperative. Model predictive control (MPC) offers a promising framework in this endeavor, providing a dynamic and forward-thinking approach [3,4]. However, the evolution to nonlinear model predictive control (NLMPC) presents an even more sophisticated means of microgrid control [5]. NLMPC not only enables anticipation and adaptation to future system behaviors but also effectively manages nonlinearities, constraints, and uncertainties inherent in microgrid operations [6,7]. The development of an effective NLMPC framework involves preserving network structure, addressing the complexities of linear and non-linear loads, and adeptly managing various resources, including energy storage devices. By seamlessly handling CPF and optimizing assets within the microgrid, NLMPC holds the potential to significantly enhance microgrid performance, promoting resilience, flexibility, and sustainability in power systems.

1.2. Literature review

The majority of distributed energy resources (DERs), which include distributed generators (DGs) and renewable energy sources (RES), are used in small electrical power grids known as microgrids (MGs). Functionally, microgrids can be categorized as either grid-connected, islanded, or in transition between these two states [2,8,9]. MPC has received significant attention in power systems engineering, particularly in MG energy management. Several factors contribute to this interest. Firstly,

* Corresponding author.
E-mail addresses: elahe.yaqubi@gmail.com (E. Yaghoubi), elnaz.yaquobi@gmail.com (E. Yaghoubi), ziyadullayusupov@karabuk.edu.tr (Z. Yusupov), cevatrahebi@topkapi.edu.tr (J. Rahebi).

https://doi.org/10.1016/j.jestch.2024.101823
Received 28 May 2024; Received in revised form 14 August 2024; Accepted 26 August 2024

Nomenclature

Abbreviations and nomenclature

PNLMPC	Proposed Nonlinear Model Predictive Control
NLMPC	Non-Linear Model Predictive Control
MIMO	Multi-Input Multiple-Output
PDF	Probability Distribution Function
MPC	Model Predictive Control
CPF	Continuous Power Flow
NPM	Network Preserving Model
BESS	Battery Energy Storage System
$u(t)$	Input Vectors
$y(t)$	Output Vectors
$\widehat{y}$	Normalized Function
f	Equality Constraint
g	Inequality Constraint
Y_{ij}	Matrix of the Connectivity between Bus i and Bus j
θ_{ij}	Voltage Angle at Bus i, j
δ_i, δ_j	Voltage Angle at Bus I and j
V_i, V_j	Voltage in bus i and bus j
I_d, I_q	Inverter's Output Current
ν_{IN}^{C}	Cut-In Wind Speed
ν_{OUT}^{C}	Cut-Out Wind Speed

MPC is well-suited for systems heavily reliant on demand and renewable energy generation forecasts, as it is based on predictions of future system behavior [10]. Secondly, the system becomes more resilient to uncertainty, as MPC provides a feedback mechanism that allows for real-time adjustments to be made [11]. Lastly, MPC effectively manages power system constraints, including generator capacity and load balance, in the tertiary control layer [12].

Numerous studies have explored the use of Model Predictive Control (MPC) for effective power system management. The Economic Model Predictive Control (EMPC) approach has gained prominence as an effective solution for optimizing economic dispatch and integrating various energy storage systems [13,14]. However, reference [13] does not consider stochastic scenarios in handling wind power uncertainty and is oblivious to market dynamics and fluctuation in pricing. Similarly, reference [14] does not deal with the issues of applying various models to predict load demand and renewable energy generation. Based on [15] the authors have suggested a real-time multi-objective load dispatch strategy for biomass heat and power cogeneration using model predictive control. While this paper gives a workable method to achieve real-time control, it overlooks operational reliability and transition times inherent in plants that convert biomass. The fact that the research does not consider independent variables that could have an impact on the performance of the proposed load dispatch control method, in view of external influences such as market dynamics or state policy changes, is overlooked. Furthermore, in reference [16], a distributed EMPC approach based on imprecise dual minimization is explored to tackle real-time economic dispatch problems. It is noteworthy, however, that the case study in this reference does not incorporate renewable generators and battery storage devices.

In this respect, the authors of reference [17] have proposed an optimization scheme for a hybrid model predictive control approach that incorporates weather prediction using the Weather Research and Forecasting (WRF) model. New rules in this setting have been introduced to deal with special needs of connection and disconnection, like minimum connection times and maximum connection frequencies. While the proposed model has been validated through simulations using real weather data, it has not yet been applied to any real microgrid. Additionally, the computational costs for this framework are high, and no provisions have been made for future policy changes related to grid connection. In [18], an approach is presented for integrating wind power into system operation in real-time using an MPC scheme, which addresses uncertainty and optimizes economic dispatch. Although it manages uncertainties in wind power, it does not sufficiently account for additional uncertainties arising from demand response programs due to the unpredictable behavior of customers. Reference [19] proposes a two-layer hierarchical approach using MPC to gain better cost savings and energy efficiency for large commercial HVAC systems. The research emphasizes the challenges of real-time control for both cost and economic dispatch problems. While this work introduces hierarchical decomposition for MPC, its evaluation is done mostly based on sample optimizations and simulation results and is lacking in terms of wide validation in the real world. As emphasized by [20], NLMPC emerges as a promising approach for real-time microgrid control, providing a specialized solution to navigate the intricate and dynamic characteristics of DERs. While NLMPC can effectively address multiple control objectives, enhancing overall microgrid operation, it's important to note that this research focuses explicitly on controlling individual microgrids rather than interconnected systems. Therefore, the NPM wasn't considered in this study. Reference [21] introduces a data-driven NLMPC framework tailored for microgrid control. This framework adeptly captures the intricate and dynamic behavior of DERs through a data-driven approach leveraging Sparse Regression (SR). It's worth noting that the accuracy of this data-driven model hinges on the quality and quantity of available data used to train the SR model. While the framework demonstrates robust performance under realistic load patterns, underscoring its relevance for practical microgrid applications, it's important to acknowledge that it does not incorporate the NPM. As noted in [22], NLMPC demonstrates its capability to efficiently manage optimal energy distribution within interconnected multi-node microgrids equipped with energy storage. By creating a virtual pool of distributed energy storage, NLMPC optimizes energy allocation and minimizes wear on storage devices. Additionally, the controller adeptly navigates diverse scenarios, including fluctuating weather conditions, varying load demands, and changing storage levels. However, it's important to note that the NPM does not directly apply in this specific context.

In research on power systems and microgrids using MPC for management and control, significant gaps remain. Table 1 compares the proposed approach with state-of-the-art techniques, emphasizing its advantages in system complexity, stability, real-time performance, and system efficiency.

Current studies often overlook essential conditions and specific network details. Most of these studies don't consider the real-life conditions of the network; they tend to stick to theoretical scenarios, which don't truly reflect the actual working conditions. Additionally, many of them prioritize cutting costs, emphasizing economic aspects, and ignoring the crucial technical and model preservation aspects of the system. This paper aims to bridge these gaps by introducing new and practical solutions to address the following shortcomings.

- Integration of a preserving network model for comprehensive system representation.
- Implementation of CPF considerations using NLMPC.
- Real-time and fast response mechanisms, improve the responsiveness of the optimal proposed NLMPC (PNLMPC) model.
- Simultaneous examination of both technical and economic aspects, ensuring a holistic understanding and optimization approach.
- The unpredictable behavior of wind speed and solar radiation is accurately modeled using the reduction technique based on Monte-Carlo Simulation.

These distinctive features underscore the novelty and superior capabilities of this research in advancing the state-of-the-art in power systems and microgrid studies.

Table 1
Comparison of Proposed Method and State-of-the-Art Techniques.

Aspect	References					This Paper
	[15]	[16]	[18]	[20]	[21]	
System Complexity	Moderate, lacks operational reliability considerations	High, but excludes renewable and storage	High, with significant computational costs	High, focused on individual microgrids	High, dependent on data quality	High, with detailed NLMPC framework
Stability	Limited, overlooks operational reliability	Limited, excludes renewable generators	Moderate, high computational costs	Advanced, but focuses on single microgrids	Advanced, depends on data-driven accuracy	Improved through PNLMPC approach
Real-Time Performance	Good, but lacks policy change considerations	Good, but lacks renewable storage integration	Moderate, not feasible for real-time due to high costs	Excellent, focuses on microgrid control	Good, depends on model quality and data	Excellent, optimized for real-time control
System Efficiency	Moderate, does not consider all operational factors	Moderate, excludes critical components	Moderate, costly and untested in practice	High, but focuses on individual systems	High, limited by data-driven model quality	High, reduces cost by significant margins

1.3. Contributions

This study introduces an innovative approach for microgrid operation, employing real-time optimal NLMPC that considers both technical and economic factors. The system's efficiency is significantly improved by utilizing a sophisticated model with diverse components and a network control strategy incorporating CPF and model preservation. Here are the primary aspects and their unique contributions:

- The study incorporates PNLMPC, which optimizes the system in real time, considering both technical and economic factors within its objective functions. This approach allows for efficient system optimization while ensuring cost-effectiveness.
- The paper employs a realistic network model that closely approximates reality, incorporating both rotating and non-rotating sources. This model accounts for uncertainties in the system and network dynamics, aiming to accurately represent the complexities of real-world systems.
- The microgrid under investigation consists of interconnected components, including wind, photovoltaic (PV), battery, and diesel systems, all interconnected with the utility grid. This interconnected setup enables seamless operation and enhances overall system stability.
- The study highlights the crucial role of the diesel generator in stabilizing power output fluctuations from primary energy generation units such as PV arrays and wind turbines. This contributes to a more stable energy supply within the microgrid.
- The mitigation of peak loads during island operations is achieved through the utilization of an Energy Storage System (ESS). This helps optimize energy usage and enhances the overall efficiency of the MG.

The approach involves utilizing CPF and applying a model preservation strategy for network control. This strategy ensures efficient and stable operation of the microgrid while preserving the integrity of the network model.

1.4. Organization

The rest of this paper is organized as follows: Section 2 explores the conceptual model, providing a comprehensive overview. The mathematical formulation of the proposed methodology is detailed in Section 3. Section 4 describes the simulation and subsequent discussion of the results derived from the simulation. The conclusive insights of this article are encapsulated in Section 5, presenting the main findings and conclusion.

2. Conceptual model overview for network dynamics

MPC incorporates diverse techniques characterized by variations in model type, objective function, and solution approach [23,24]. Various MPC formulations can be employed for effective MG management [25]. In this study, NLMPC serves as a central controller, regulating each resource by adjusting the load under varying network conditions. This controller supervises technical aspects and optimizes critical parameters like frequency and voltage, as depicted in Fig. 1, while simultaneously minimizing costs.

Fig. 1 illustrates the NLMPC as the central controller in an islanded microgrid. The microgrid includes a mix of rotating and non-rotating resources, including photovoltaic panels, wind turbines, diesel generation, and battery storage. The NLMPC optimizes power flows and control setpoints among various DGs and loads. The configuration comprises three inverters dedicated to the photovoltaic system, wind turbines and battery storage, a diesel generator, and local loads. Moreover, the diesel generator is directly connected to the MG. In this setup, Inverter 1 (associated with the photovoltaic system) acts as the PV bus, and Inverter 2 serves as the V/F bus, and Inverter 3 (associated with battery storage) functions as the PQ bus when in charging mode and as the PV bus when in discharging mode. The NLMPC manages the operation of the inverters and the diesel generator to ensure that power generation meets load demand while maintaining the required voltage and frequency levels.

2.1. Optimal NLMPC control methodology

The NLMPC is a key component of the microgrid and is responsible for coordinating the operation of various DGs and loads to achieve optimal control. Using a nonlinear model-based approach, the NLMPC effectively anticipates and manages the dynamic behavior of microgrids. It optimizes power flow between DGs and loads, minimizing energy losses. Moreover, the NLMPC enhances adaptability by incorporating uncertainty models to forecast variable renewable energy sources and load fluctuations, thereby improving system resilience. This framework keeps on performing optimally with changes in DG addition or load variations. As a central control element, the NLMPC manages the operation of all microgrid components, maintaining voltage and frequency stability, optimizing energy efficiency, and ensuring a reliable power supply to the loads. Given that energy storage is a pivotal component of MGs, their dynamic models are commonly expressed as state-space equations, with the state variable x(t) representing the charge level of the batteries. This implies that state-space models can effectively define the predictive control problem, rendering state-space MPC a promising choice for an islanded MG management. Moreover, this formulation is well-suited for handling multi-variable systems, a common scenario in an islanded MG. To model the behavior of a linear system, the following equations are employed:

$$\begin{cases} \mathrm{X}(t+1) = \mathrm{A}x(t) + \mathrm{B}u(t) \\ y(t) = Cx(t) \end{cases} \tag{1}$$

MGs are often multi-input multiple-output (MIMO) systems. MIMO systems have m-dimensional input vectors u(t) and n-dimensional

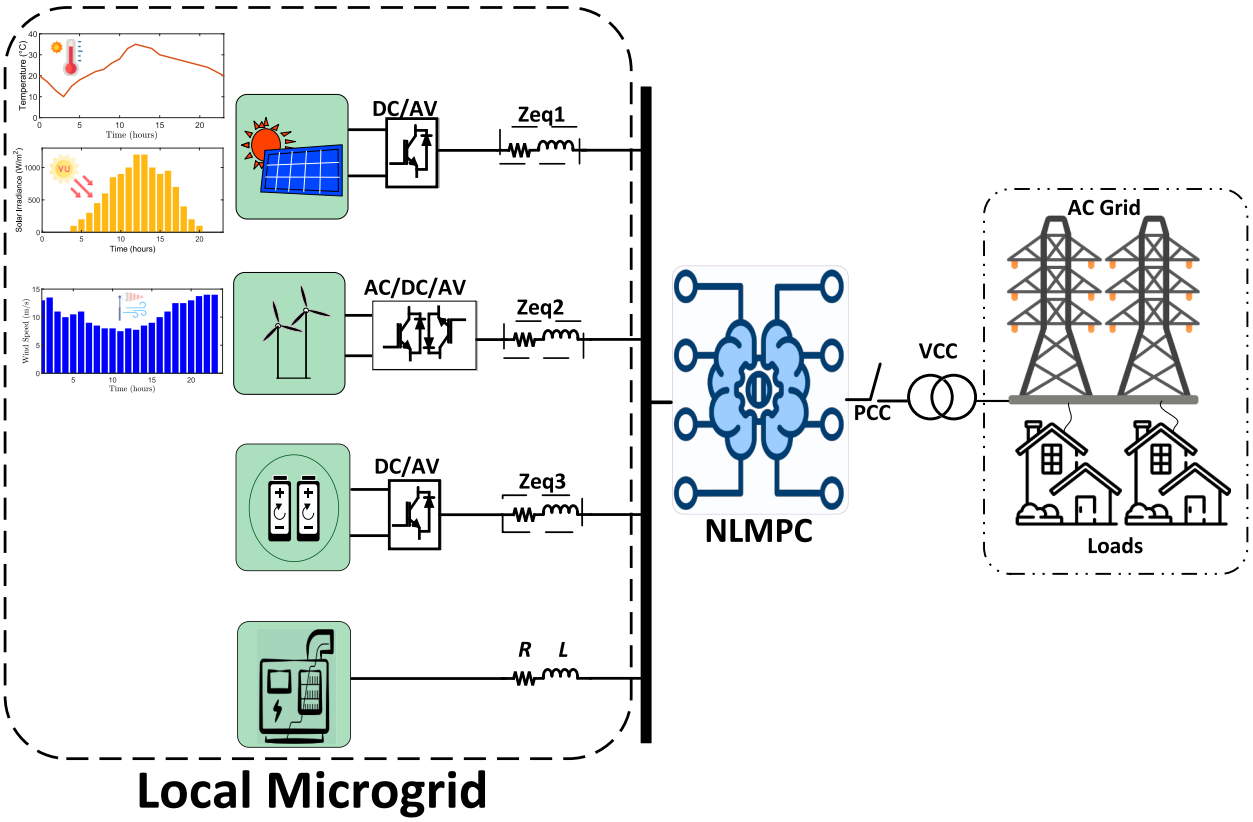

Fig. 1. Conceptual model of network and islanded MG.

output vectors y(t). Matrix C equals identity because the output y(t) typically follows the state X(t) [26]. MPC computes a future control sequence over a finite horizon by utilizing the system's current state, input, and output measurements, along with its model at each sampling instant. This control series meets constraints on the control action while optimizing a specified performance index. The control goal is to identify a series of control inputs across a specific prediction horizon, based on the current measurement, that satisfies a particular objective function and constraints. The control sequence described above will provide a predicted series of state vectors, which may be utilized to compute the expected sequence of system outputs. With the use of this knowledge, the system may be controlled, and the procedure is then repeated with the state measurement of the following time step acting as an initial condition to calculate the control input. Typically, the major objective is to penalize the control effort required to achieve the future output by tracking a certain reference signal along the prediction horizon. Hence, the following mathematical explanation of the MPC's objective function and constraints are possible:

$$\min J(\mathrm{N}_p) = \sum_{j=1}^{\mathrm{N}_p} \left[\| \hat{y}(t+j|t) - r(t+j) \|_R^2 + \| \Delta u(t+j-1) \|_Q^2 \right] \tag{2}$$

$$s.t: \begin{cases} f(\hat{y}_t^j, \hat{x}_t^j, \hat{u}_t^j) = 0 \\ g(\hat{y}_t^j, \hat{x}_t^j, \hat{u}_t^j) \leqslant 0 \end{cases} \tag{3}$$

Where, the $\hat{y}$ is a normalized function encompassing various objectives, including voltage optimization, frequency management, power losses reduction, and cost minimization for the network. R and Q are diagonal positive definite weighting matrices, and functions f and g indicates the equality and inequality constraints, respectively [27].

Hence, the objective function for the PNLMPC problem would be:

$$\min J(\mathrm{N}_p) = \sum_{j=1}^{\mathrm{N}_p} \left[\| \hat{y}(t+j|t) - r(t+j) \|_R^2 + \| \Delta u(t+j-1) \|_Q^2 \right] + [c\hat{y}(t+j|t)]] \tag{4}$$

where c represents the contribution cost for the state variables [28], and the constraints would be the same as regular MPC. In fact, the objective function incorporates all technical and economic parameters and conducts optimization accordingly. Additional details regarding these aspects will be presented in the subsequent sections.

3. Problem formulation

This section outlines the goals and limitations of the proposed algorithm. The objective functions revolve around technical considerations, including power loss, operating cost, frequency and voltage stability, voltage deviation, and the management of storage devices. Following this, the section delves into the mathematical formulations and constraints associated with modeling both rotating and non-rotating resources. In the context of real-time applications, a method's efficacy is measured by its ability to promptly estimate stability margins without relying on post-fault information, coupled with a low computational cost. However, from a real-time perspective, recalculating the system's operating point becomes challenging and time-consuming due to system topology changes resulting from disturbances. Network reduction models were prevalent in the initial stages of direct method development. In the 1980s, the concept of NPMs emerged to overcome the drawbacks associated with network-reduction models [29]. By employing a NPM, the network structure is conserved, leading to the designation of the corresponding NLMPC function as a "structure-preserving" energy function. In direct comparison with network-reduction models, Network-preserving models offer several advantages for direct

stability analysis [30–32]:

In system modeling, it preserves the original network topology, allowing for a more realistic representation of power system components, including dynamic load behavior (voltage and frequency variations) at load buses and detailed generator models.
In terms of the energy function, the transfer conductance of the preserving model significantly outperforms that of network-reduction models. This results in a numerical energy function that closely approximates the exact energy function.
From a computational standpoint, sparse matrix techniques can efficiently solve the nonlinear algebraic equations involved in the model.

In this study, the network-preserving model employs CPF, which is implemented through equations (5) and (6).

$$P_i = \sum_{j=1}^{n} |V_i||V_j||Y_{ij}|\cos(\theta_{ij} - \delta_i + \delta_j) \tag{5}$$

$$Q_i = -\sum_{j=1}^{n} |V_i||V_j||Y_{ij}|\sin(\theta_{ij} - \delta_i + \delta_j) \tag{6}$$

where, Y_{ij} is the matrix representing the connectivity between bus i and bus j.

The PNLMPC framework is specifically designed to address the inherent uncertainties in microgrid operation, including variations in renewable energy generation, unpredictable load changes, and potential equipment failures. As Fig. 2 depicts an inverter model with an LC filter, the PNLMPC employs a model-based predictive control strategy. This strategy relies on a nonlinear mathematical model of the islanded microgrid to forecast and optimize system behavior over a future time horizon. By incorporating the nonlinear dynamics of various components—such as inverters, the diesel generator, and energy storage—the PNLMPC captures complex interactions more effectively and makes more informed control decisions. The optimization process accounts for factors like renewable energy availability, battery state-of-charge, load forecasts, and system constraints, aiming to achieve objectives such as cost minimization, emissions reduction, and enhanced reliability. This system operates under slower droop control, as shown in Fig. 3.

The effective terminal voltage and phase angle of the inverter, post-LC filter passage, are denoted as $U\angle\varphi$ in accordance with this model. By employing this representation, system dynamics can be accurately characterized using the inverter's terminal states (angle, frequency, and voltage) and the line currents as dynamic variables without the necessity of considering the internal states of the inverter. This methodology is based on a 5th-order electromagnetic (EM) model, encompassing three inverter-related states (angle, frequency, and voltage) and two line-related states (the two components of the current phasor). The equations detailing this model in the dq reference frame are as follows:

$$\dot{\varphi} = \varpi - \varpi_0 \tag{7}$$

$$\tau\dot{\varpi} = \varpi_{set} - \varpi - \frac{\Re_p \varpi_0}{\zeta_n} P_{measurment} \tag{8}$$

$$\tau\dot{U} = U_{set} - U - \frac{\Re_q}{\zeta_n} Q_{measurment} \tag{9}$$

$$L\dot{I}_d = U_{\cos\theta} - U_0 - RI_d + \varpi_0 LI_d \tag{10}$$

$$L\dot{I}_d = U_{\sin\theta} - U_0 - RI_d + \varpi_0 LI_d \tag{11}$$

In this context, the variables U and φ represent the effective terminal voltage and phase angle of the inverter, respectively, once they pass through the LC filters. The variable ϖ denotes the frequency of the inverter. Additionally, the variables I_d and I_q represent the dq-frame components of the inverter's output current. The equations (8) and (9) describe the behavior of the terminal voltage and frequency, respectively. These equations incorporate the influence of low-pass filters in the inverter power control system, which is characterized by the bandwidth $\varpi_c = \tau - 1$, and the values of $\Re_p$ and $\Re_q$ are the frequency and voltage droop gains, respectively.

Moreover, ζ_n denotes the inverter rating, while ϖ_{set} and U_{set} are the set points of frequency and voltage controllers, respectively, and they are considered as inputs of the inverter. It is noteworthy that both ϖ and ϖ_0 are considered to be measured in rad/s. The expressions for $P_{mearsurment}$ and $Q_{mearsurment}$ are given by $P_{mearsurment} = \frac{3}{2}UI_d$ and $Q_{mearsurment} = \frac{3}{2}UI_q$.

On the other hand, equations (10) and (11) capture the electromagnetic dynamics of the complex current $I(t)$. The variables $L = L_c + L_l$

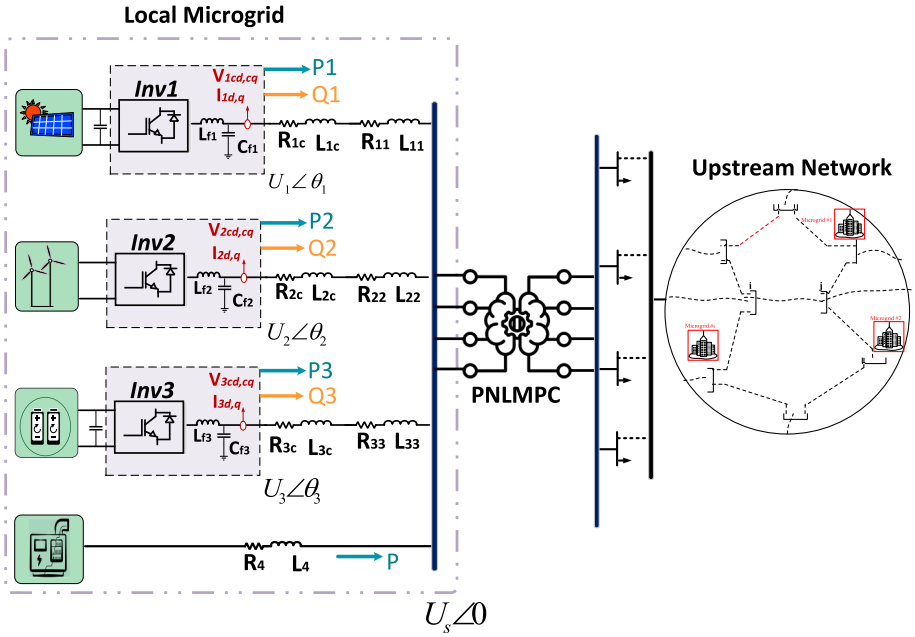

Fig. 2. Illustration of the studies inverter model.

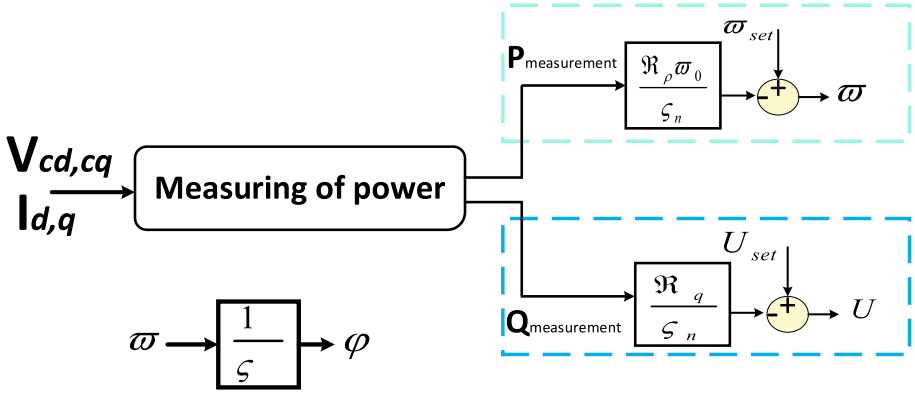

Fig. 3. The inverter droop controller.

and $R = R_c + R_l$ represent the combined inductance and resistance of the connection, respectively, as observed at the inverter terminal.

3.1. Modeling of photovoltaic panels

Through the utilization of photovoltaic panels, the generation of power can be assessed utilizing the equation:

$$P_{PV}^{t,S}\left(SR^{t,S}\right) = N_{PV} \times FF \times V^{t,S} \times I^{t,S} \begin{cases} \{\forall t \in \mathrm{T} \\ \forall s \in S \end{cases} \tag{12}$$

The generation of electricity through photovoltaic panels $P_{PV}^{t,S}$ relies on changes in solar radiation $SR^{t,S}$, ambient temperature $A\mathrm{T}^{t}$,time t based on hours, and particular scenario (s). A comprehensive examination of these factors, along with other pertinent attributes, is thoroughly discussed in the reference [33].

$$\begin{cases} FF = \dfrac{V_{MPP} \times I_{MPP}}{V_{OC} \times I_{SC}} \\ V^{t,S} = V_{OC} - K\nu\left(A\mathrm{T}^{t} + SR^{t,S}\left(\dfrac{N_{OT} - 20}{0.8}\right)\right) \\ I^{t,S} = SR^{t,S}\left[I_{SC} + K\nu\left(\mathrm{T}^{t,S} - 25\right)\right] \end{cases} \tag{13}$$

3.2. Modeling of wind turbine

The power produced by a wind turbine depends on both the wind speed and the specific type of wind turbine, as described by the following equation [34].

$$P_{Wind\ \mathrm{turbine}}^{T,S}\left(\nu_{T,S}\right): \begin{cases} 0 \rightarrow if \begin{cases} \nu_{T,S} \leqslant \nu_{IN}^{C} \\ or \\ \nu_{T,S} \geqslant \nu_{OUT}^{C} \end{cases} \\ \alpha + \beta \times \nu_{T,S} + \gamma \times \left(\nu_{T,S}\right)^2 \rightarrow if \begin{cases} \nu_{IN}^{C} \leqslant \nu_{T,S} < \nu_{R} \\ \nu_{R} \leqslant \nu_{T,S} < \nu_{OUT}^{C} \end{cases} \end{cases} \tag{14}$$

where $P_{Wind\ \mathrm{turbine}}^{T,S}$ represents the generated power, and ν_{IN}^{C} denotes the cut-in wind speed, indicating the lower threshold at which the wind turbine can generate power. Conversely, ν_{OUT}^{C} represents the cut-out wind speed, signifying the upper limit beyond which the wind turbine stops generating power to prevent potential damage. Moreover, α, β, and γ collectively represent the coefficients of the wind turbine. Various wind turbine models may employ distinct mathematical expressions derived from empirical data and theoretical considerations.

3.3. Modeling of BESS

The comprehensive modeling approach for the ESS addresses considerations for its integration and performance within the MG. This involves utilizing a set of specified equations, including equations (7) to (11), along with equations (15) and (16).

$$P_{Ch}, P_{Dis} = \pm\left(\frac{3}{2}U_d I_d\right) \tag{15}$$

$$\dot{E} = \eta . P_{Ch} \tag{16}$$

Where $\dot{E}$ represents rate of change of battery energy and η shows the coulombic efficiency. The energy stored in the battery can be calculated using the following expression:

$$E_B(t) = \begin{cases} E_B(t-1) + \left(\dfrac{\dot{E}}{\Delta T}\right) - \left(\dfrac{\mathrm{P}_{B(t)}^{Dis}}{\Delta T}\right).\left(\dfrac{1}{\eta_B^{Dis}}\right) & t > 1 \\ E_B(0) + \left(\dfrac{\dot{E}}{\Delta T}\right) - \left(\dfrac{\mathrm{P}_{B(t)}^{Dis}}{\Delta T}\right).\left(\dfrac{1}{\eta_B^{Dis}}\right) & t = 1 \end{cases} \tag{17}$$

Where $E_B(t)$ (kWh) represents the battery's energy level at time t, and $E_B(0)$ denotes the initial energy level of the battery. Notably, the charging and discharging operations of the battery energy storage system (BESS) do not occur simultaneously, so binary variables $\Im_B^{Ch}$ and $\Im_B^{Dis}$ are employed for operational decision-making. Additionally, the binary variables constrain the BESS charging/discharging capacity. Considering the constraints posed by degradation, equation (21) sets limits on the BESS's lower and upper energy levels.

$$0 \leqslant \mathrm{P}_{B(t)}^{Ch} \leqslant \mathrm{P}_{B,\max}^{Ch} . \Im_B^{Ch} \tag{18}$$

$$0 \leqslant \mathrm{P}_{B(t)}^{Dis} \leqslant \mathrm{P}_{B,\max}^{Dis} . \Im_B^{Dis} \tag{19}$$

$$\Im_B^{Ch} + \Im_B^{Dis} \leqslant 1 \tag{20}$$

$$E_{B,\min} \leqslant E_B(t) \leqslant E_{B,\max} \tag{21}$$

$$\dot{SoC} = \frac{\dot{E}}{E} \tag{22}$$

$\dot{SoC}$ relates the rate of change of state of charge and the total battery energy is described by E.

3.4. Modeling of diesel generator

Alterations in active power have a substantial impact on the overall

system frequency, with reactive power displaying a comparatively lower sensitivity to frequency variations, predominantly depending on changes in voltage magnitude. As a result, active and reactive power are managed by distinct control mechanisms. The load frequency control (LFC) loop oversees active power and frequency, while the automatic voltage regulator (AVR) loop maintains control over reactive power and voltage magnitude. The importance of LFC has grown with the expansion of interconnected systems, facilitating their efficient operation. In this study, our focus is exclusively on the LFC loop for generators, while the AVR loop is disregarded. Consequently, it is assumed that the diesel generator solely contributes to the distribution of active power. LFC is implemented for every generator in a connected power system. Fig. 4 illustrates the diagram depicting the LFC loop. The controllers are configured based on a specific operational state and are responsible for managing slight changes in load requirements to ensure that the frequency remains within predefined boundaries. Minor changes in active power are predominantly influenced by alterations in the rotor angle, subsequently impacting the frequency.

The explanation of the primary components of LFC, including the Governor, prime mover load, and rotating mass model, is provided as follows:

1) The Governor model: the input command ΔP_G is converted via a hydraulic amplifier into the steam valve position ΔP_V. The governor time constant T_G characterizes the response time of the governor, and its transfer function is given by:

$$\frac{\Delta P_V(s)}{\Delta P_G(s)} = \frac{1}{1 + T_G s} \tag{23}$$

2) Prime mover model: the prime mover model serves the purpose of generating mechanical power, which can be accomplished through the utilization of various energy sources such as steam for steam turbines or water for hydraulic turbines. The prime mover model, denoted as $\Delta P_{mechanical}$, establishes a relationship between the mechanical power output and variations in the steam valve position ΔP_V. The transfer function for this model is expressed as:

$$\frac{\Delta P_V(s)}{\Delta P_G(s)} = \frac{1}{1 + T_{Turbin} s} \tag{24}$$

3) Rotating mass and load model: the response of the motor load to changes in frequency can be assessed through the examination of its speed-load characteristic.

$$\frac{\Delta\varpi(s)}{\Delta P_{mechanical}(s) - \Delta P_{Load}(s)} = \frac{1}{2Hs + D} \tag{25}$$

Utilizing equations (23), (24), and (25), the LFC loop for the diesel generator can be constructed, as depicted in Fig. 5.

The s-domain equations describing the block diagram can be expressed as:

$$\begin{cases} (1 + T_{Turbin}s)\Delta P_V(s) = \Delta P_{reference} - \dfrac{1}{R}\Delta\varpi(s) \\ (1 + T_{Turbin}s)\Delta P_{mechanical}(s) = \Delta P_V \\ (2Hs + D)\Delta\varpi(s) = \Delta P_{mechanical} - \Delta P_{Load} \end{cases} \tag{26}$$

$$\begin{cases} s\Delta P_V(s) = -\dfrac{1}{T_G}\Delta P_V(s) - \dfrac{1}{RT_G}\Delta\varpi(s) + \dfrac{1}{T_G}\Delta P_{reference}(s) \\ s\Delta P_{mechanical}(s) = \dfrac{1}{T_{Turbin}}\Delta P_V(s) - \dfrac{1}{T_T}\Delta P_{mechanical}(s) \\ s\Delta\varpi(s) = \dfrac{1}{2H}\Delta P_{mechanical}(s) - \dfrac{D}{2H}\Delta\varpi(s) - \dfrac{1}{2H}\Delta P_{Load}(s) \end{cases} \tag{27}$$

Transforming into time-domine, it is observed that:

$$\begin{cases} \dot{\Delta P}_V(s) = -\dfrac{1}{T_G}\Delta P_V - \dfrac{1}{RT_G}\Delta\varpi + \dfrac{1}{T_G}\Delta P_{reference} \\ \dot{\Delta P}_{mechanical}(s) = \dfrac{1}{T_{Turbin}}\Delta P_V - \dfrac{1}{T_{Turbin}}\Delta P_{mechanical} \\ \dot{\Delta\varpi} = \dfrac{1}{2H}\Delta P_{mechanical} - \dfrac{D}{2H}\Delta\varpi - \dfrac{1}{2H}\Delta P_{Load} \end{cases} \tag{28}$$

where in our study, $[\Delta P_V, \Delta P_{mechanical}, \Delta\varpi]^T$ are states of the diesel generator and ΔP_{Load} is the input of the system. Expressing in matrix form, with $\Delta P_{reference} = 0$, the state equation becomes:

$$\begin{bmatrix} \dot{\Delta P}_V \\ \dot{\Delta P}_{mechanical} \\ \dot{\Delta\varpi} \end{bmatrix} = \begin{bmatrix} \dfrac{-1}{T_G} & 0 & \dfrac{1}{RT_G} \\ \dfrac{1}{T_{Turbine}} & \dfrac{-1}{T_{Turbine}} & 0 \\ 0 & \dfrac{1}{2H} & \dfrac{-D}{2H} \end{bmatrix} \begin{bmatrix} \Delta P_V \\ \Delta P_{mechanical} \\ \Delta\varpi \end{bmatrix} + \begin{bmatrix} 0 \\ 0 \\ \dfrac{-1}{2H} \end{bmatrix} [\Delta P_{Load}] \tag{29}$$

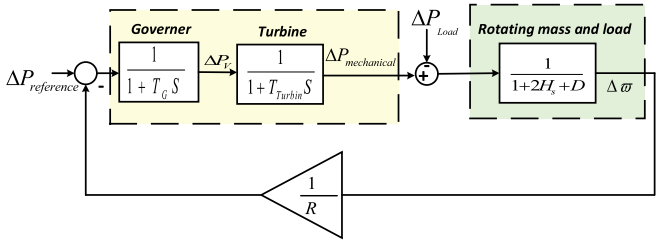

Fig. 5. Load frequency control of diesel generator.

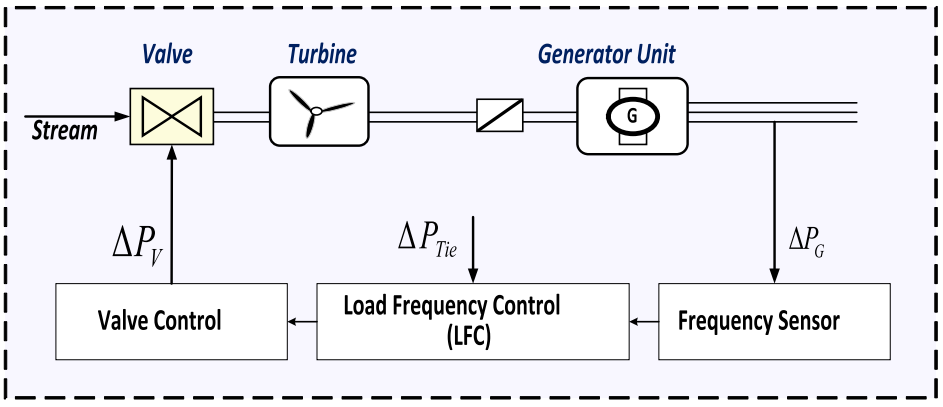

Fig. 4. Block diagram of automatic LFC.

3.5. Control oriented model

Fig. 6 depicts the microgrid configuration under investigation, comprising three inverter-based DERs and a diesel generator, forming an island microgrid. It is crucial to highlight that the system comprises a total of 20 dynamical equations, with 7 inputs and 7 outputs. Therefore, the entire system can be formulated as follows:

elements $[\omega_{set2}, u_{set2}]^T$, administering control signals for its operation. Moreover, the vector $[u_5(\kappa), u_6(\kappa)]^T$ is specific to inverter 2 with elements $[\omega_{set3}, u_{set3}]^T$, providing control signals for its operation. The input $u_7^T(\kappa)$ is responsible for controlling the diesel generator, which is equal to P_L.

*Inverter*1 :

$$\begin{aligned}\chi_1(\kappa+1) &= f_1(\chi(\kappa))\\ \chi_2(\kappa+1) &= f_2(\chi(\kappa), u(\kappa))\\ \chi_3(\kappa+1) &= f_3(\chi(\kappa), u(\kappa))\\ \chi_4(\kappa+1) &= f_4(\chi(\kappa))\\ \chi_5(\kappa+1) &= f_5(\chi(\kappa))\end{aligned}$$

*Inverter*2 :

$$\begin{aligned}\chi_6(\kappa+1) &= f_6(\chi(\kappa))\\ \chi_7(\kappa+1) &= f_7(\chi(\kappa), u(\kappa))\\ \chi_8(\kappa+1) &= f_8(\chi(\kappa), u(\kappa))\\ \chi_9(\kappa+1) &= f_9(\chi(\kappa))\\ \chi_{10}(\kappa+1) &= f_{10}(\chi(\kappa))\end{aligned}$$

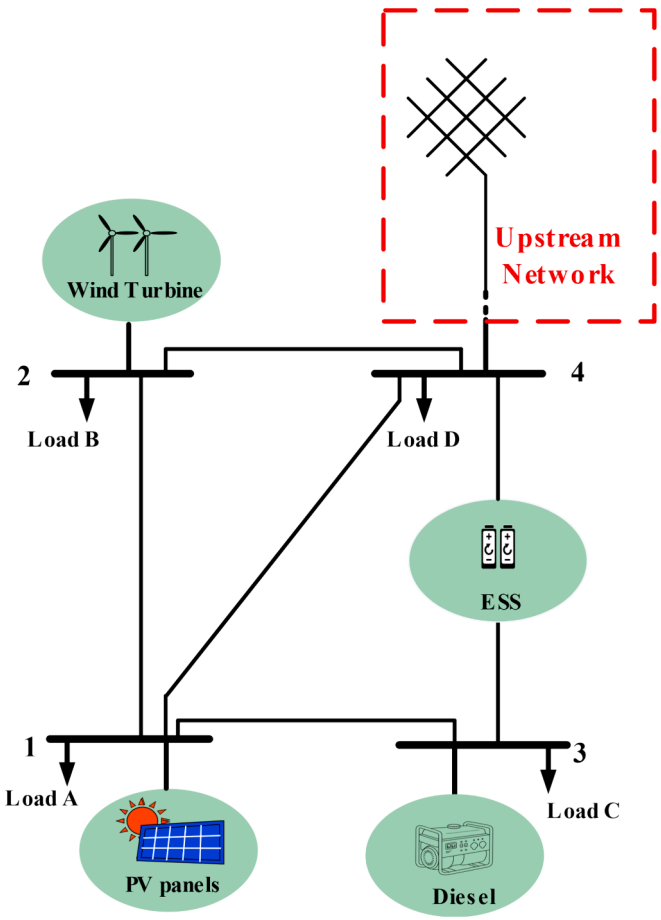

Fig. 6. Illustration of the schematic of microgrid under investigation.

*Inverter*3 :

$$\begin{aligned}\chi_{11}(\kappa+1) &= f_{11}(\chi(\kappa))\\ \chi_{12}(\kappa+1) &= f_{12}(\chi(\kappa))\\ \chi_{13}(\kappa+1) &= f_{13}(\chi(\kappa), u(\kappa))\\ \chi_{14}(\kappa+1) &= f_{14}(\chi(\kappa))\\ \chi_{15}(\kappa+1) &= f_{15}(\chi(\kappa), u(\kappa))\\ \chi_{16}(\kappa+1) &= f_{16}(\chi(\kappa), u(\kappa))\\ \chi_{17}(\kappa+1) &= f_{17}(\chi(\kappa))\end{aligned}$$

DieselGenerator :

$$\begin{aligned}\chi_{18}(\kappa+1) &= f_{18}(\chi(\kappa))\\ \chi_{19}(\kappa+1) &= f_{19}(\chi(\kappa))\\ \chi_{20}(\kappa+1) &= f_{20}(\chi(\kappa))\end{aligned} \tag{30}$$

where,

$$\begin{cases}\chi(\kappa) = \left[\chi_1^T(\kappa), \chi_2^T(\kappa), \chi_3^T(\kappa), \ldots, \chi_{20}^T(\kappa)\right]^T\\ u(\kappa) = \left[u_1^T(\kappa), u_2^T(\kappa), u_3^T(\kappa), \ldots, u_7^T(\kappa)\right]^T\end{cases} \tag{31}$$

In the considered context, the state vector $[\chi_1(\kappa), \ldots, \chi_5(\kappa)]^T$ with elements $\left[\theta_1(\kappa), \omega_1(\kappa), u_1(\kappa), I_{d1}(\kappa), I_{q1}(\kappa)\right]^T$ represents the dynamic variables of inverter number one. Similarly, the state vector $[\chi_6(\kappa), \ldots, \chi_{10}(\kappa)]^T$ with elements $\left[\theta_2(\kappa), \omega_2(\kappa), u_2(\kappa), I_{d2}(\kappa), I_{q2}(\kappa)\right]^T$ corresponds to inverter number two. The state vector $[\chi_{11}(\kappa), \ldots, \chi_{15}(\kappa)]^T$ with elements $\left[\theta_3(\kappa), \omega_3(\kappa), u_3(\kappa), I_{d3}(\kappa), I_{q3}(\kappa)\right]^T$ corresponds to inverter number three. Furthermore, the state vector $[\chi_{16}(\kappa), \ldots, \chi_{20}(\kappa)]^T$ represents the state variables $[P_v, P_m, \omega_d]^T$ of the diesel generator.

Regarding control inputs, the vector $[u_1(\kappa), u_2(\kappa)]^T$ is linked to inverter 1, controlling its operation with elements $[\omega_{set1}, u_{set1}]^T$. The vector $[u_3(\kappa), u_4(\kappa)]^T$ is designated for inverter 2 featuring elements $[\omega_{set2}, u_{set2}]^T$, administering control signals for its operation. Moreover, the vector $[u_5(\kappa), u_6(\kappa)]^T$ is specific to inverter 2 with elements $[\omega_{set3}, u_{set3}]^T$, providing control signals for its operation. The input $u_7^T(\kappa)$ is responsible for controlling the diesel generator, which is equal to P_L.

3.6. Cost modeling

The formulations of cost models for photovoltaic panels (PV), wind turbines, battery energy storage system (BESS), diesel generators, and the grid are expressed in equations (32) to (37). For comprehensive explanations of the symbols and variables used in these equations, please refer to references [35–37].

$$COST^{\varsigma}(t) = A_{\varsigma} + B_{\varsigma} \times P^{p}(t) \begin{cases} \forall t \in \\ \forall \varsigma \in [PV, Wind\ \text{turbine}] \end{cases} \tag{32}$$

$$A_{\varsigma} = \frac{COST_{capital}^{\varsigma} \times P_{capital}^{\varsigma} \times AIR}{T_{life} \times 365 \times 24 \times CF_{\varsigma}}; B_{\varsigma} = COST_{\varsigma}^{O\&M} \rightarrow \forall \varsigma \in [PV, Wind\ \text{turbine}] \tag{33}$$

$$COST^{BESS}(t) = A_{BESS} + B_{BESS} \times \left|P^{BESS}(t)\right| \pm \beta^{TOU}(t) \times P^{BESS}(t) \rightarrow \forall t \in T \tag{34}$$

$$A_{BESS} = \frac{COST_{capital}^{BESS} \times P_{capital}^{BESS} \times AIR}{T_{life} \times 365 \times 24 \times CF_{BESS}}; \rightarrow B_{BESS} = COST_{BESS}^{O\&M} \tag{35}$$

$$\begin{cases} COST^{\varsigma} = COST_{O\&M}^{\varsigma}(t) + H_{\varsigma} \times COST_{EMI}^{\varsigma}(t) \\ COST_{O\&M}^{\varsigma}(t) = c + b \times P_{\varsigma}(t) + a \times P_{\varsigma}^2(t) \\ COST_{EMI}^{\varsigma}(t) = \left(C_{CO_2}^{\varsigma} + C_{SO_2}^{\varsigma} + C_{NO_2}^{\varsigma}\right) \times P_{\varsigma}(t) \end{cases} \rightarrow \forall \varsigma \in \{DiselGenerator, Grid\}, \forall t \in T \tag{36}$$

$$H_{\varsigma} = \frac{COST^{\varsigma}_{O\&M}(t)}{COST^{\varsigma}_{EMI}(t)}\Big|_{P^{MAX}_{\varsigma}} \rightarrow \forall \varsigma \in \{DiselGenerator, Grid\}, \forall t \in T \quad (37)$$

Where,A_{ς} is Capital cost component. The $COST^{\varsigma}_{capital}$ is the initial investment in the system. B_{ς} is operational and Maintenance (O&M) cost component. $COST^{O\&M}_{\varsigma}$ are ongoing costs for running and maintaining the system. $COST^{\varsigma}_{EMI}$ is Emission cost. H_{ς} is emission factor.

3.7. Modeling uncertainty

The unpredictable characteristics of wind power generation and photovoltaic systems present a challenge in microgrid operation. Neglecting uncertainty issues leads to unrealistic and inaccurate model results. To address this, a stochastic model based on scenario generation and reduction has been employed to improve the module's reliability and mitigate uncertainties associated with PV and WT. The uncertainty associated with solar radiation is typically addressed by fitting its probability distribution using the beta Probability Distribution Function (PDF):

$$PDF(x) = \frac{\wp(\alpha+\beta)}{\wp(\alpha)+\wp(\beta)} \times x^{\alpha-1} \times (1-x)^{\beta-1} \quad (38)$$

where, α and β are determined from the mean value ϑ, and the standard deviation using equation (39).

$$\beta = (1-\vartheta) \times \left(\frac{\vartheta(1-\vartheta)}{\delta^2} - 1\right), \alpha = \frac{\vartheta \times \beta}{1-\vartheta} \quad (39)$$

Additionally, the uncertain behavior of wind is commonly described using the Weibull distribution function. Further details regarding modeling and parameter selection are available in [33].

$$PDF(v) = \frac{k}{c}\left(\frac{v}{c}\right)^{\beta-1} \exp\left(-\left(\frac{v}{c}\right)^{k}\right) \Rightarrow k = \left(\frac{\delta}{c}\right)^{k}; c = \frac{\vartheta}{\wp\left(1+\frac{1}{k}\right)} \quad (40)$$

where, k and c represent the shape and scale parameters for the Weibull function, respectively.

After generating scenarios, a backward scenario reduction technique is applied [33]. Initially, the interval for each pair of scenarios is calculated. Subsequently, for each scenario, the one with the shortest distance is determined. The closest match for each scenario is identified by multiplying the probability of scenarios occurring at the distance of the scenario's closest match. The scenario with the least impact is identified and eliminated.

4. Simulation results

In this section, the PNLMPC is simulated by MATLAB 2023a. The simulation employs the NLMPC toolbox provided by MATLAB Simulink on a PC running Windows 10 Pro, equipped with an Intel Corei7-6500U processor clocked at 2.50 GHz and 12.0 GB of RAM.

4.1. Input parameters of the system

Fig. 6 presents a schematic diagram of the microgrid under study, highlighting its interconnected DGs. Figs. 7, 8, and 9 illustrate the uncertainties associated with wind speed, solar radiation, and ambient temperature, respectively. These uncertainties are modeled using PDF to accurately capture the variability in these parameters.

In an islanded microgrid, which operates independently from the main grid, fluctuations in wind and solar power due to weather uncertainties can significantly impact system stability and reliability. These variations in power generation may lead to voltage and frequency instability, complicating load management. Additionally, uncertainties in ambient temperature can influence the efficiency and output of generating units. To address these challenges, the microgrid design should integrate energy storage solutions, such as batteries, to mitigate the variability in renewable power generation. Furthermore, the control and energy management system must be designed to accommodate the dynamic nature of renewable energy production and ensure stable operation of the microgrid.

Moreover, loads within a microgrid exhibit variability and uncertainties due to factors such as changes in consumer behavior, weather conditions, and fluctuations in load demand. Figs. 10 and 11 illustrate these uncertainties in both active and reactive loads, simulated using probability density functions (PDF). The peaks of the PDF curves represent the load magnitudes with the highest probability of occurrence during microgrid operation. This information is crucial for understanding the dynamic behavior of the microgrid and its response to load changes. Insights from Figs. 10 and 11 can inform the design and operation of the microgrid, including energy storage system sizing, optimization of control strategies, and evaluation of system stability and resilience.

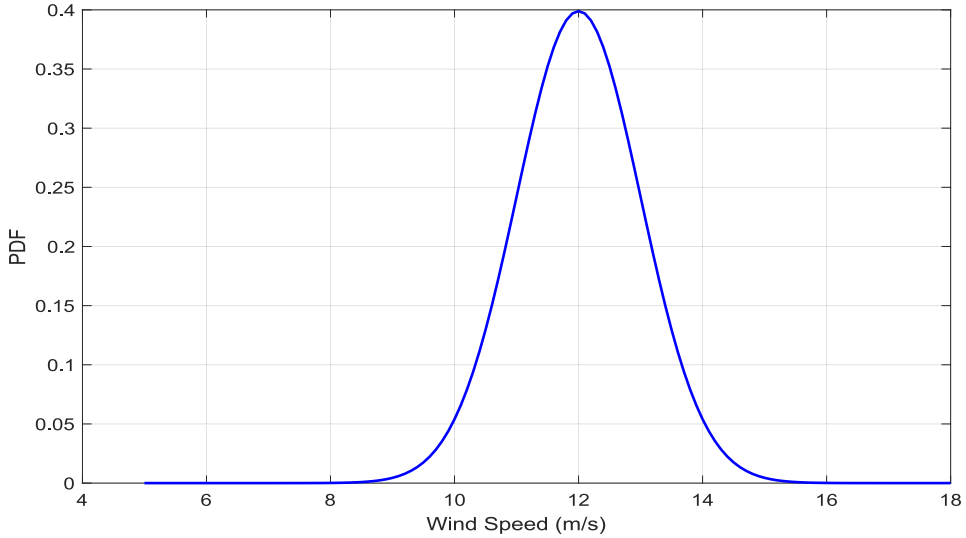

Fig. 7. The PDF of nominal wind speed variations during operation of MG.

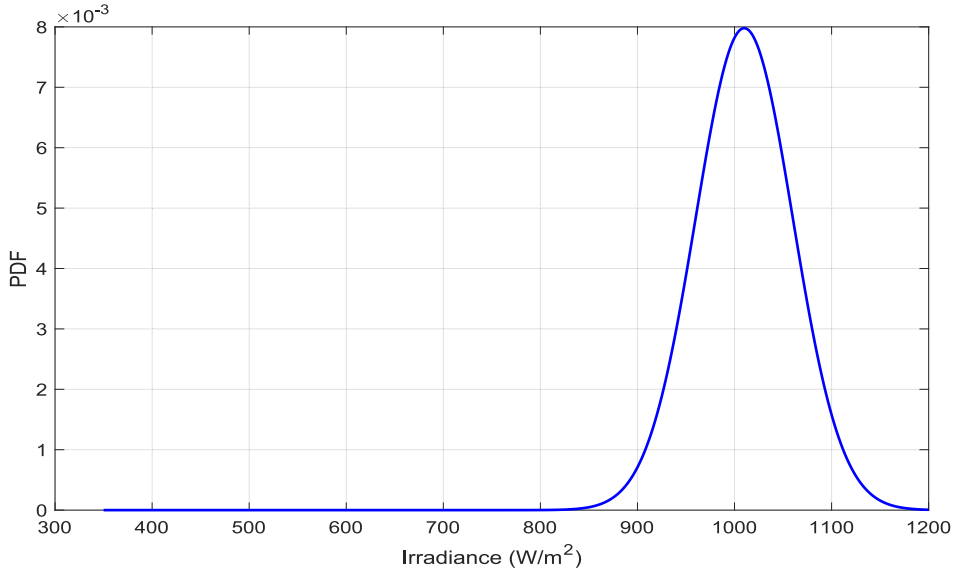

Fig. 8. The PDF of nominal Irradiance variations during operation of MG.

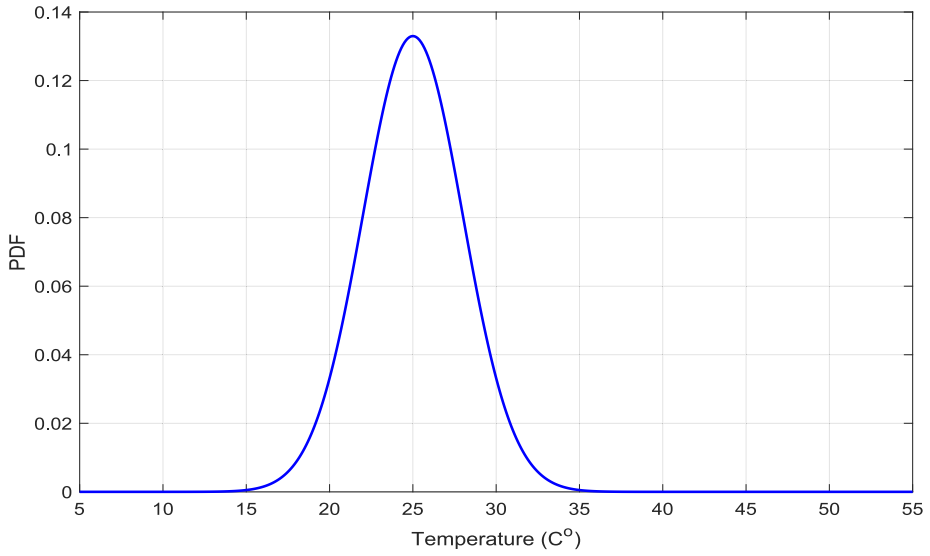

Fig. 9. The PDF of nominal temperature variations during operation of MG.

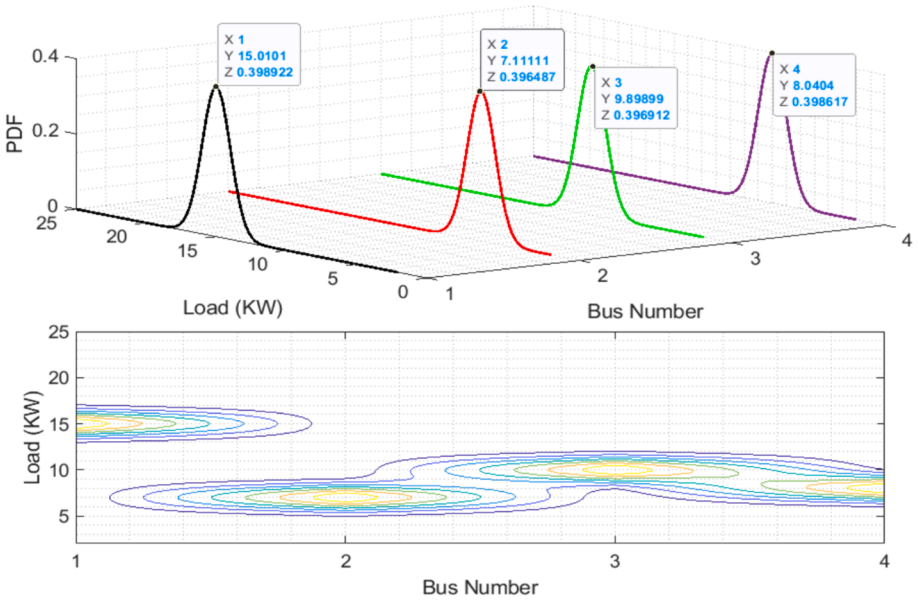

Fig. 10. The PDF of nominal active load variations during operation of MG.

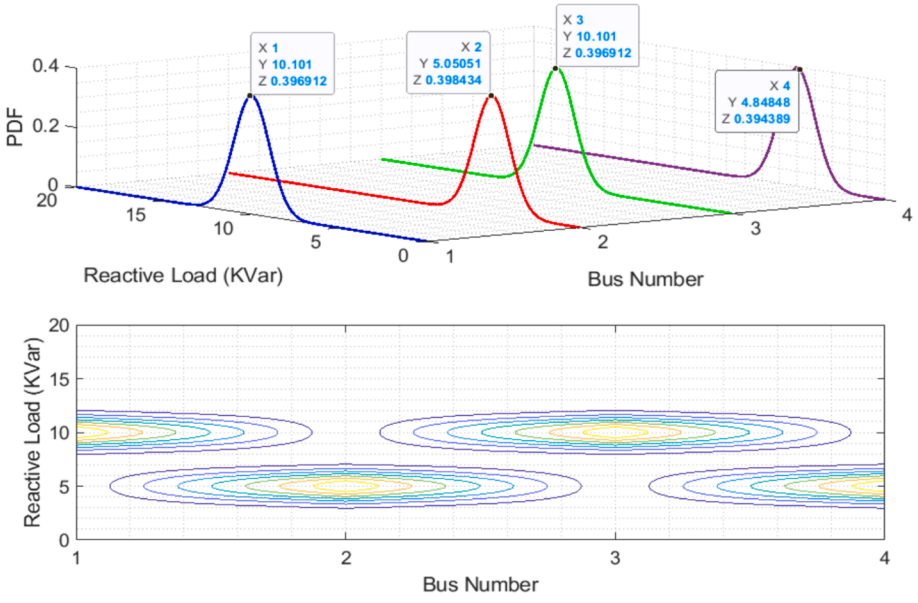

Fig. 11. The PDF of nominal reactive load variations during operation of MG.

4.2. Results and analysis

Figs. 12 and 13 depict a continuous-time representation of active and reactive power. In Fig. 12, the green line represents the active power reference, while the purple line illustrates the combined active power generated from all microgrid DGs. Notably, at the 15th second, the active power dynamically transitions from 40 kW to 130 kW. The PNLMPC adjusts the DGs to ensure that the summation of generated active powers closely follows the active power reference with high accuracy and speed. This results in a balanced relationship, where the sum of generated active power corresponds to the sum of active power consumption.

Furthermore, in Fig. 13, the reactive power reference is denoted by the pink line, and the blue line represents the summation of generated reactive power from all DGs in the microgrid. Significantly, at the 22nd second, the reactive power dynamically shifts from 30 kVAR to 40 kVAR. The NLMPC regulates the DGs to guarantee that the total generated reactive power closely tracks the reactive power reference with precision and speed. This leads to an equilibrium where the total amount of generated reactive power corresponds with the total amount of reactive power consumption. Figs. 14-17 provide a detailed insight into the optimal output of active power from individual DGs within the microgrid. The PV panel and wind turbine showcase their optimal generation in green and purple, respectively, while the diesel generator and battery storage indicate their optimal active power generating rates in grey (Fig. 16) and red (Fig. 17).

Fig. 17 specifically highlights the active power generated by the battery storage system. Initially, negative active power during the first 10 s signifies the battery being in a charging state. Once reaching full charge, the battery ceased to receive power input from the 10th to the 15th second. However, a substantial surge in active power consumption, from 40 kW to 130 kW at the 15th second, triggered the battery to

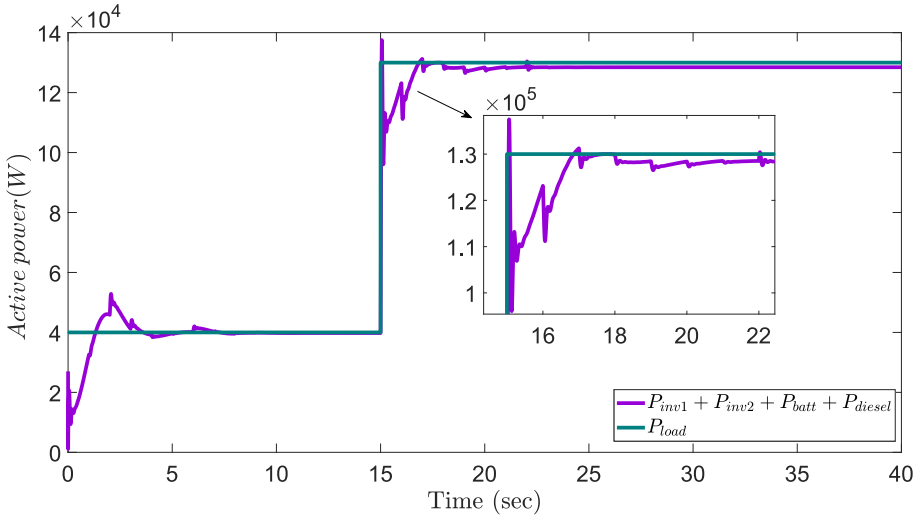

Fig. 12. Active power dynamics in the microgrid, regulated for balance by MPC.

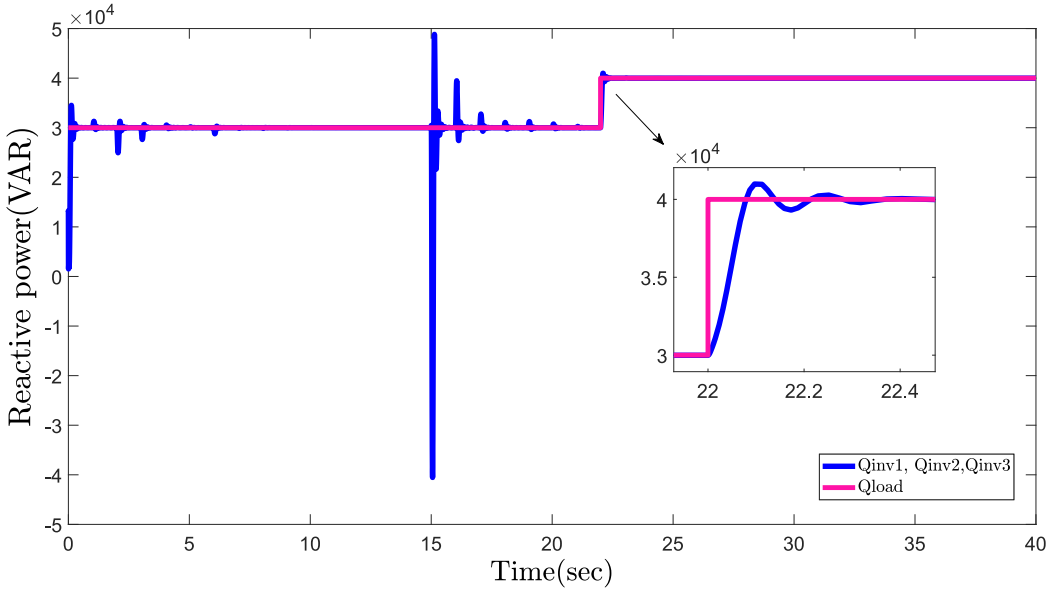

Fig. 13. Reactive power dynamics in the microgrid, regulated for balance by MPC.

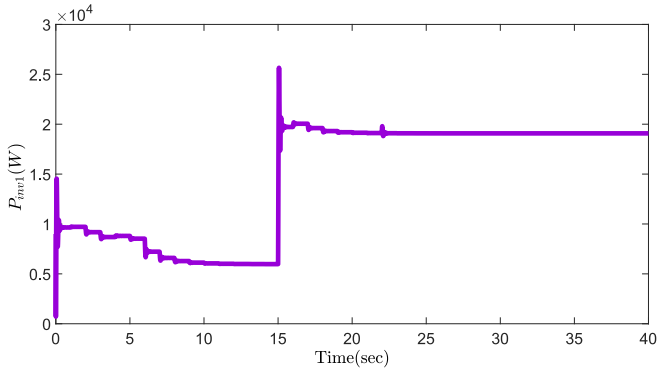

Fig. 14. Peak of active power generation from PV panels.

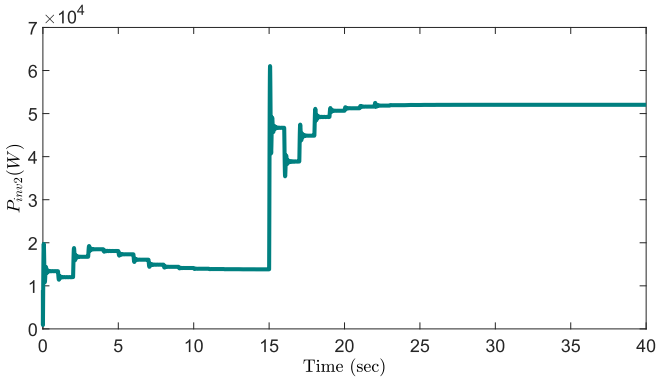

Fig. 15. Peak of active power generation from wind turbine.

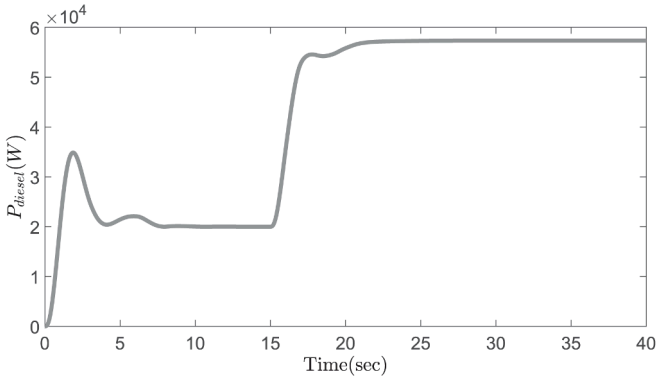

Fig. 16. Peak active power generation from diesel generator.

commence discharging, exhausting its stored energy by the 20th second. Consequently, by the 25th second, the battery ceased supplying any additional active power to the microgrid. In the event of the battery being unable to provide active power to the microgrid, inverters 1 and 2 sequentially intervene to compensate, as depicted in Figs. 14 and 15. Particularly noteworthy is, initiating an escalation in active power production to regulate voltage and frequency. This compensation mechanism ensures a delicate balance between total active power consumption and generation, as demonstrated in Fig. 15. Commencing from the 20th second onwards, there's a concerted effort towards both voltage and frequency control, coupled with optimizing the economic efficiency of the microgrid to maintain network stability.

Fig. 18 provides an overview of the battery storage status managed by PNLMPC, initially charged to 20 Wh (equivalent to 25% State of Charge). The battery's protective range is set between 100% and 25%. As shown in Fig. 15, during the initial 15 s, with low active power, the battery underwent a steady charging process, reaching full capacity at 100% or 80 Wh. However, at the 15th second, with a sharp increase in active power from 40 kW to 130 kW, the battery discharged to support the microgrid, reaching a discharge level of 25%. This discharge strategy ensures the protection of the storage device, preventing deep discharge as per the limitations of the protection system.

Frequency characteristics (in rad/sec) of inverters 1, 2, and the BESS are displayed in Fig. 19. These results unequivocally showcase the efficacy of our proposed method in consistently upholding stable frequency levels, even amidst fluctuations in both active and reactive power.

Fig. 20 presents a comparative analysis examining voltage performance across different control methods. Specifically, three distinct controllers are evaluated for voltage stability: the PNLMPC, depicted by a black line; a standard MPC, represented by a blue line; and an adaptive MPC, illustrated with a red line. The voltage level is standardized at 380 V in this experimental setup. It's evident that the PNLMPC exhibits superior control before any significant changes. Moreover, at the 15th (sec) time interval, amidst an escalation in active power demand, the PNLMPC, indicated by the black line, demonstrates the most effective voltage regulation during this period. Furthermore, it swiftly converges to the reference value after that, while the remaining controllers fail to track the reference closely. Notably, the voltage fluctuates between 381.6 V and 382.2 V before and after the fluctuation in the PNLMPC. At the same time, the range for the adaptive MPC spans from 383.5 V to 387.7 V, and the reference targets cannot be met. Similarly, the standard MPC struggles to adhere to the references, registering 385.5 V before the fluctuation and reaching 396.6 V post-fluctuation.

Moreover, optimization extends beyond technical parameters to encompass economic considerations for validation during the operational phase. Hence, the PNLMPC controller is tasked with adjusting generation to minimize all operational costs arising from sudden changes. In Fig. 21, three different controllers are analyzed: the PNLMPC (depicted by the black line), the standard MPC (shown in red), and the adaptive MPC (represented by the blue line). Before any shifts in active power, costs are uniform across all controllers. However, at the 15th moment, when a sudden load increase occurs, the PNLMPC swiftly adapts generation to minimize operational costs, displaying superior speed and accuracy compared to its counterparts. Additionally, as

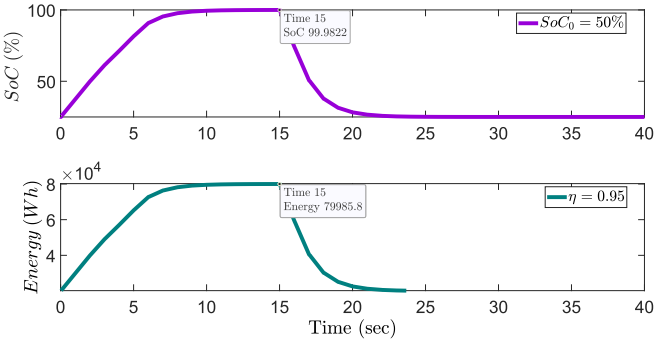

Fig. 18. PNLMPC −managed battery storage dynamics.

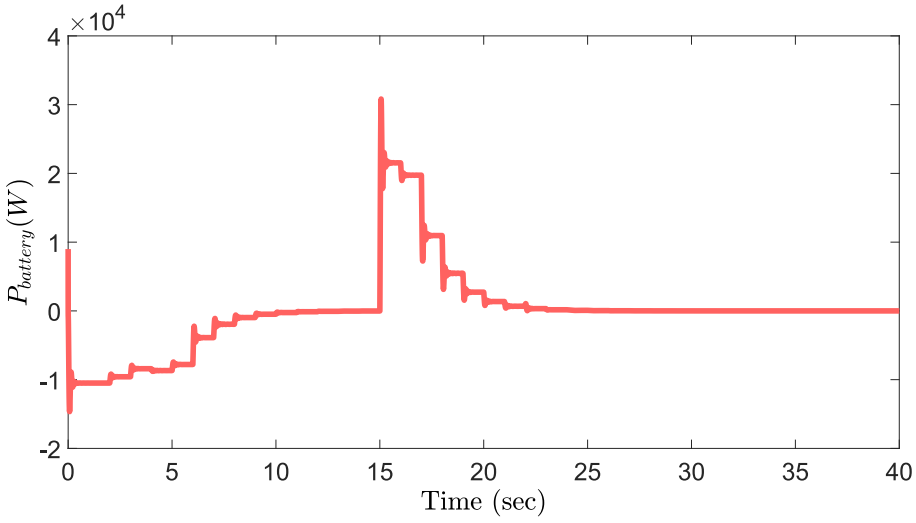

Fig. 17. Peak active power generation from battery storage.

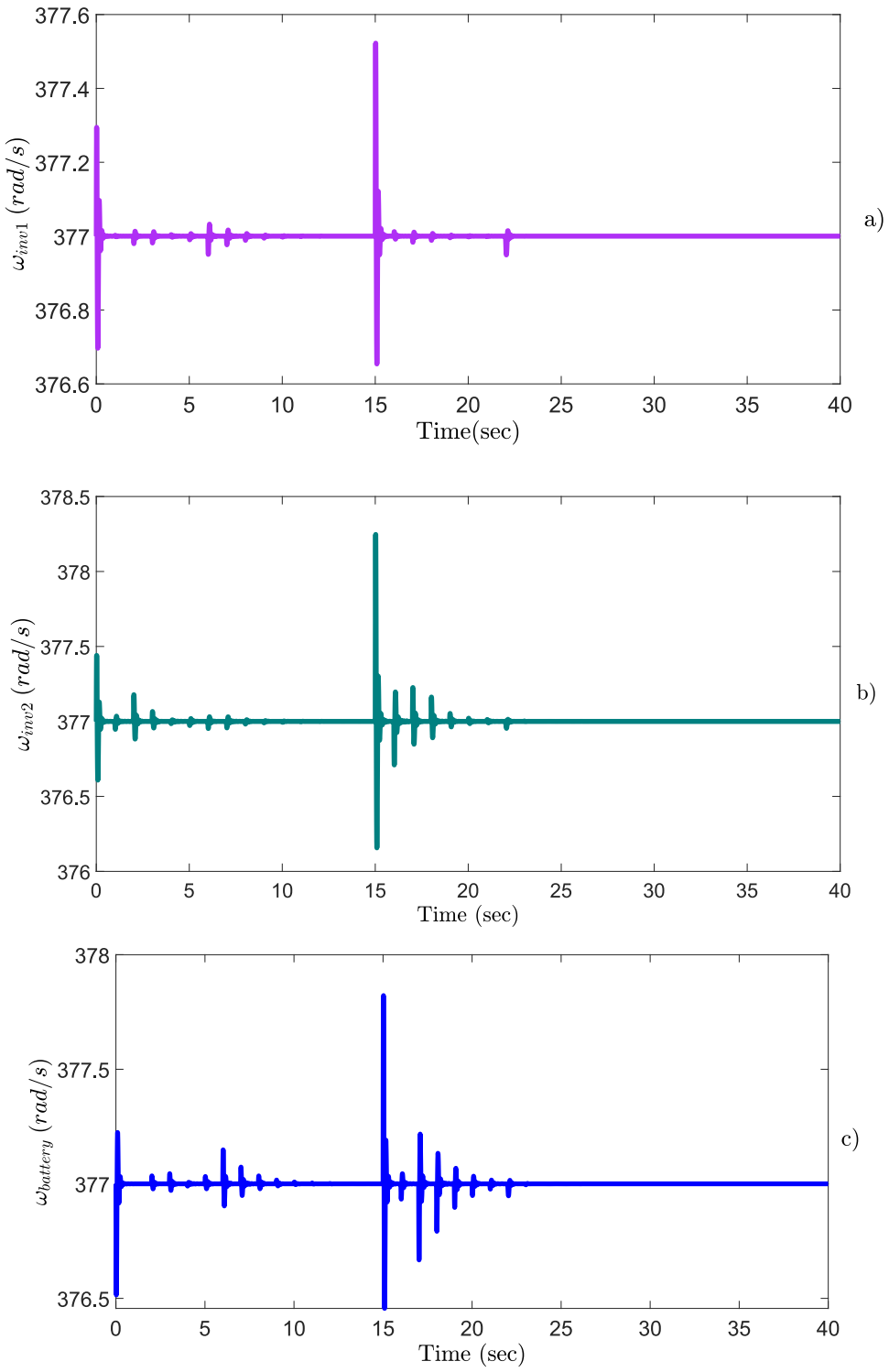

Fig. 19. Stable frequency control amidst Power Fluctuations with PNLMPC. a) controlling the frequency of photovoltaic systems (inverter 1). b) controlling the frequency of wind turbine (inverter 2). c) controlling the frequency of BESS (inverter 3).

evident from the magnified section of Fig. 21, the PNLMPC consistently causes lower costs throughout the system's startup phase than alternative controllers. Following load increases and stabilization of inverters, the PNLMPC system continually adjusts distributed generation capacity to minimize operational expenses. Given the significant load increase at the 15th moment, the discrepancy in operational costs becomes more pronounced.

Table 2 has been compiled for a comparative analysis between PNLMPC and alternative methodologies as part of our validation efforts. The results of optimizing the objective function using PNLMPC and other methods are presented. The proposed optimization algorithm consistently outperforms its counterparts across all metrics,

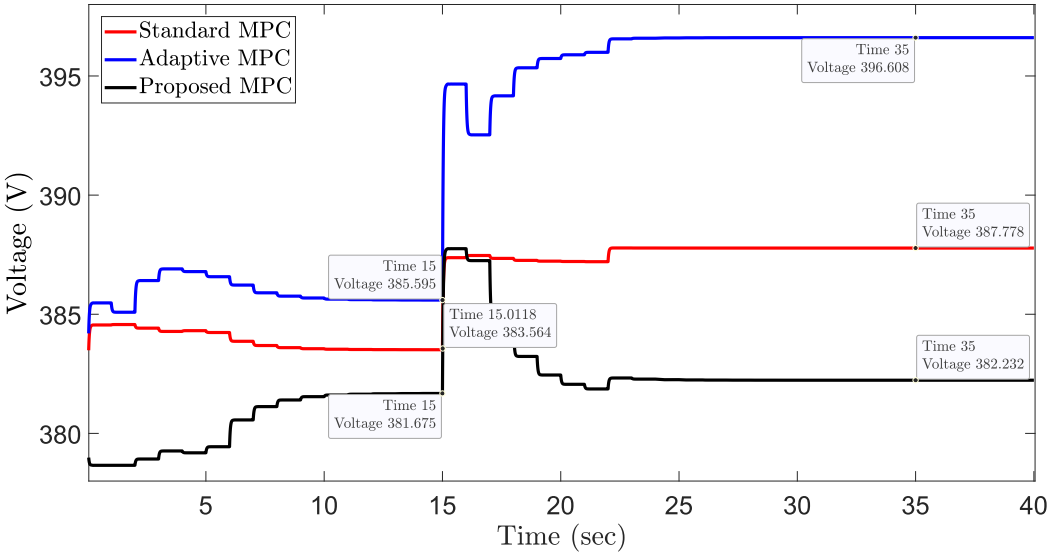

Fig. 20. Comparative analysis of voltage stability across PNLMPC, Standard MPC, and Adaptive MPC.

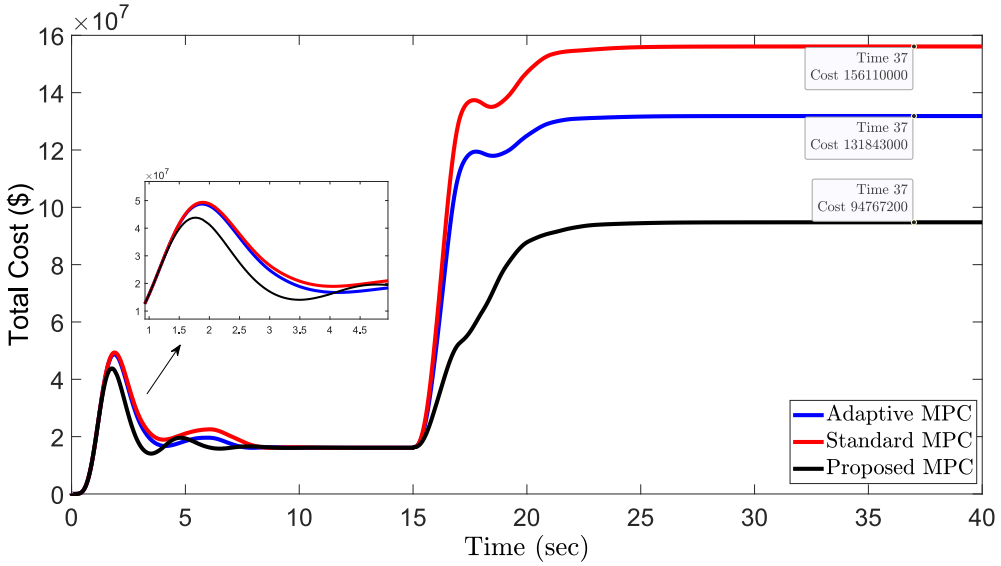

Fig. 21. Comparative analysis of economic parameter optimization for PNLMPC, Standard MPC, and Adaptive MPC.

demonstrating superior performance. To ensure fairness, the results from other methodologies were implemented by us, using the same objective function and parameters as in the original papers. A fixed number of problem evaluations were allocated to all methods to ensure a meaningful comparison and control for computational cost differences. All methodologies addressed the same optimization problem, enabling a direct assessment of PNLMPC's performance. This systematic evaluation aimed to discern each method's relative strengths and weaknesses, providing valuable insights into their practical applicability for the same task.

Table 2 clearly illustrates that the difference in cost savings between the Standard MPC and Adaptive MPC is around 15.54%. Additionally, the PNLMPC reduced costs by 39.29% compared to the Standard MPC and by 28.12% compared to the Adaptive MPC. Furthermore, PNLMPC shows significantly lower total voltage deviation and frequency deviation compared to both Standard MPC and Adaptive MPC, with values of 0.26% and 0.00045%, respectively. In terms of total voltage deviation, PNLMPC achieves an outstanding reduction of 85.87% and 87.62% compared to Standard MPC and Adaptive MPC, respectively. Similarly, PNLMPC demonstrates remarkable improvements of 99.46% and 96.62% in frequency deviation compared to Standard MPC and Adaptive MPC, respectively. Additionally, PNLMPC demonstrates the shortest

Table 2
Comparative analysis between PNLMPC and alternative methodologies for validation.

Consideration Statues	Operating Cost ($)	Total Voltage Deviation (%)	Frequency Deviation (%)	CPU-Time for 40(sec) Simulation
PNLMPC	94,767,200	0.26	0.00045	39.4
Standard MPC [38,39]	156,110,000	1.84	0.0832	600
Adaptive MPC [40,41]	131,843,000	4.2	0.0173	1125

CPU-Time for 40 s of simulation, showcasing its efficiency in convergence and calculation, thus highlighting the effectiveness of the proposed framework in real-time applications.

5. Conclusions

Managing real-time control in islanded microgrids, considering the system's dynamics and components alongside the NPM is a multifaceted endeavor requiring a nuanced blend of technical acumen and economic prudence. This paper introduces a novel framework aimed at addressing these challenges, offering solutions to optimize system performance within technical and economic constraints. By integrating NPM and CPF within a platform based on NLMPC, the proposed framework presented a comprehensive strategy for efficiently managing network parameters while meeting real-time objectives. The study underscores the importance of grappling with uncertainties inherent in generation and consumption resources, advocating for a realistic portrayal of microgrid dynamics. Simulation results, closely resembling real-world scenarios, affirm the efficacy and versatility of the proposed framework in optimizing the output generation of various resources, thereby enhancing both the technical and economic aspects of the system. Notably, the proposed framework meticulously considers the dynamics of the network and its components, along with their associated uncertainties. Through the optimization function embedded within the PNLMPC framework, crucial network parameters such as frequency and voltage are effectively managed, addressing real-time economic and technical objectives simultaneously. When compared to Standard MPC and Adaptive MPC, the proposed PNLMPC approach demonstrates superior performance in both technical and economic aspects. Although Adaptive MPC performs better than Standard MPC technically, the analysis reveals that PNLMPC excels in both voltage and frequency regulation, maintaining minimal deviations before and after fluctuations. Regarding total voltage deviation, PNLMPC achieves a remarkable decrease of 85.87% and 87.62% in comparison to Standard MPC and Adaptive MPC, respectively. Likewise, PNLMPC exhibits impressive enhancements of 99.46% and 96.62% in frequency deviation compared to Standard MPC and Adaptive MPC, respectively. Economically, while Standard MPC can reduce costs by up to 15.54% compared to Adaptive MPC, PNLMPC significantly outperforms both, reducing costs by 39.29% compared to Standard MPC and by 28.12% compared to Adaptive MPC. Furthermore, the integration of CPF and the NPM yields a model that faithfully mirrors real-world conditions, providing an accurate representation of island microgrid dynamics. The experimental results indicate that PNLMPC exhibits the shortest CPU-Time for simulation compared to both Standard MPC and Adaptive MPC. This emphasizes the effectiveness of the proposed framework for real-time applications. Thus, by employing this holistic methodology, the proposed approach significantly contributes to the advancement of more effective management strategies for practical microgrid applications. Looking ahead, further research and implementation of our framework hold promise for bolstering the resilience and efficiency of microgrid systems in response to evolving energy challenges.

6. Future direction

Future research will concentrate on advancing the scalability and computational efficiency of the PNLMPC framework to ensure its applicability to larger and more complex microgrid systems. While this study has primarily focused on islanded mode operations, subsequent investigations will expand the framework's applicability to grid-connected microgrids. Additionally, future work will assess the impact of economic factors and policy changes on the PNLMPC framework's performance. This will involve simulating various market conditions and regulatory scenarios to determine their effects on the framework's efficiency and cost-effectiveness.

Compliance with ethical standards

CRediT authorship contribution statement

Elaheh Yaghoubi: Writing – review & editing, Writing – original draft, Visualization, Validation, Supervision, Software, Resources, Project administration, Methodology, Investigation, Funding acquisition, Formal analysis, Data curation, Conceptualization. **Elnaz Yaghoubi:** Visualization, Validation, Software, Methodology, Formal analysis, Conceptualization. **Ziyodulla Yusupov:** Writing – review & editing, Visualization. **Javad Rahebi:** Writing – review & editing, Visualization.

Declaration of Competing Interest

The authors declare that they have no known competing financial interests or personal relationships that could have appeared to influence the work reported in this paper.

References

[1] Z. Yusupov, N. Almagrahi, E. Yaghoubi, E. Yaghoubi, A. Habbal, and D. Kodirov, "Modeling and Control of Decentralized Microgrid Based on Renewable Energy and Electric Vehicle Charging Station." pp. 96-102.
[2] R. Wazirali, E. Yaghoubi, M.S.S. Abujazar, R. Ahmad, A.H. Vakili, State-of-the-art review on energy and load forecasting in microgrids using artificial neural networks, machine learning, and deep learning techniques, Electr. Pow. Syst. Res. 225 (2023) 109792.
[3] H.S. Khan, K. Kauhaniemi, Design and FPGA-in-loop based validation of predictive hierarchical control for islanded AC microgrid, Eng. Sci. Technol, Int. J. 48 (2023) 101557.
[4] S.R. Cominesi, M. Farina, L. Giulioni, B. Picasso, R. Scattolini, A two-layer stochastic model predictive control scheme for microgrids, IEEE Trans. Control Syst. Technol. 26 (1) (2017) 1–13.
[5] F. Garcia-Torres, A. Zafra-Cabeza, C. Silva, S. Grieu, T. Darure, A. Estanqueiro, Model predictive control for microgrid functionalities: Review and future challenges, Energies 14 (5) (2021) 1296.
[6] J. Hu, Y. Shan, J.M. Guerrero, A. Ioinovici, K.W. Chan, J. Rodriguez, Model predictive control of microgrids–An overview, Renew. Sustain. Energy Rev. 136 (2021) 110422.
[7] A. Nurkanović, A. Mešanović, A. Zanelli, G. Frison, J. Frey, S. Albrecht, and M. Diehl, "Real-time nonlinear model predictive control for microgrid operation." pp. 4989-4995.
[8] S. Saha, S. Gholami, M.K.K. Prince, Sensor fault-resilient control of electronically coupled distributed energy resources in islanded microgrids, IEEE Trans. Ind. Appl. 58 (1) (2021) 914–929.
[9] Z. Yusupov, E. Yaghoubi, V. Soyibjonov, Reducing the vulnerability in microgrid power systems, Sci. Innovat. 2 (A5) (2023) 166–175.
[10] F. Langner, W. Wang, M. Frahm, V. Hagenmeyer, Model predictive control of distributed energy resources in residential buildings considering forecast uncertainties, Energ. Buildings 303 (2024) 113753.
[11] M. Çetin, B. Bahtiyar, S. Beyhan, Adaptive uncertainty compensation-based nonlinear model predictive control with real-time applications, Neural Comput. Appl. 31 (2019) 1029–1043.
[12] O. Babayomi, Z. Zhang, T. Dragicevic, R. Heydari, Y. Li, C. Garcia, J. Rodriguez, R. Kennel, Advances and opportunities in the model predictive control of microgrids: Part II–Secondary and tertiary layers, Int. J. Electr. Power Energy Syst. 134 (2022) 107339.
[13] C. Huang, Y. Zong, S. You, C. Træholt, Economic model predictive control for multi-energy system considering hydrogen-thermal-electric dynamics and waste heat recovery of MW-level alkaline electrolyzer, Energ. Conver. Manage. 265 (2022) 115697.
[14] I. Brahmia, J. Wang, L. de Oliveira, H. Xu, Hierarchical smart energy management strategy based on cooperative distributed economic model predictive control for multi-microgrids systems, Int. Trans. Electr. Energy Syst. 31 (2) (2021) e12732.
[15] L. Li, D. He, J. Jin, B. Yu, X. Gao, Multi-objective load dispatch control of biomass heat and power cogeneration based on economic model predictive control, Energies 14 (3) (2021) 762.
[16] J. Köhler, M. A. Müller, F. Allgöwer, N. Li, "Distributed Economic Model Predictive Control for Achieving Real-time Economic Dispatch with Frequency Control in Power Systems," 2019.
[17] D.P. e Silva, J.L.F. Salles, J.F. Fardin, M.M.R. Pereira, Management of an island and grid-connected microgrid using hybrid economic model predictive control with weather data, Appl. Energy 278 (2020) 115581.
[18] F. Arasteh, G.H. Riahy, MPC-based approach for online demand side and storage system management in market based wind integrated power systems, Int. J. Electr. Power Energy Syst. 106 (2019) 124–137.
[19] J.B. Rawlings, N.R. Patel, M.J. Risbeck, C.T. Maravelias, M.J. Wenzel, R.D. Turney, Economic MPC and real-time decision making with application to large-scale HVAC energy systems, Comput. Chem. Eng. 114 (2018) 89–98.

[20] D.F. Pereira, F. da Costa Lopes, E.H. Watanabe, Nonlinear model predictive control for the energy management of fuel cell hybrid electric vehicles in real time, IEEE Trans. Ind. Electron. 68 (4) (2020) 3213–3223.
[21] M. Shadaei, J. Khazaei, F. Moazeni, Data-driven nonlinear model predictive control for power sharing of inverter-based resources, IEEE Trans. Energy Convers. (2024).
[22] D. Trigkas, C. Ziogou, S. Voutetakis, S. Papadopoulou, Virtual energy storage in RES-powered smart grids with nonlinear model predictive control, Energies 14 (4) (2021) 1082.
[23] I. Harbi, J. Rodriguez, E. Liegmann, H. Makhamreh, M.L. Heldwein, M. Novak, M. Rossi, M. Abdelrahem, M. Trabelsi, M. Ahmed, Model predictive control of multilevel inverters: challenges, recent advances, and trends, IEEE Trans. Power Electron. (2023).
[24] A. Castelletti, A. Ficchì, A. Cominola, P. Segovia, M. Giuliani, W. Wu, S. Lucia, C. Ocampo-Martinez, B. De Schutter, J.M. Maestre, Model Predictive Control of water resources systems: a review and research agenda, Annu. Rev. Control. (2023).
[25] A. Topa, J. Gil, J. Álvarez, J. Torres, A hybrid-MPC based energy management system with time series constraints for a bioclimatic building, Energy 287 (2024) 129652.
[26] C. Bordons, F. Garcia-Torres, M.A. Ridao, Model predictive control of microgrids, Springer (2020).
[27] E. Mayhorn, K. Kalsi, J. Lian, M. Elizondo, "Model predictive control-based optimal coordination of distributed energy resources." pp. 2237-2244.
[28] R. Halvgaard, N. K. Poulsen, H. Madsen, J. B. Jørgensen, "Economic model predictive control for building climate control in a smart grid." pp. 1-6.
[29] H.-D. Chiang, Direct methods for stability analysis of electric power systems: theoretical foundation, BCU methodologies, and applications: John Wiley & Sons, 2011.
[30] K. Padiyar, K. Ghosh, Direct stability evaluation of power systems with detailed generator models using structure-preserving energy functions, Int. J. Electr. Power Energy Syst. 11 (1) (1989) 47–56.
[31] N. Narasimhamurthi, M. Musavi, A generalized energy function for transient stability analysis of power systems, IEEE Trans. Circuits Systems I Fund. Theory Appl. 31 (7) (1984) 637–645.
[32] M.Z. Jahromi, S.M. Kouhsari, A novel recursive approach for real-time transient stability assessment based on corrected kinetic energy, Appl. Soft Comput. 48 (2016) 660–671.
[33] A. Azizi, H. Karimi, S. Jadid, Daily operation of multi-energy systems based on stochastic optimization considering prediction of renewable energy generation, IET Renew. Power Gener. 16 (2) (2022) 245–260.
[34] A.F. Zobaa, S.A. Aleem, Uncertainties in modern power systems, Academic Press, 2020.
[35] A. A. Abou El-Ela, R. A. El-Sehiemy, A.-M. Kinawy, and E. S. Ali, "Optimal placement and sizing of distributed generation units using different cat swarm optimization algorithms." pp. 975-981.
[36] T. Niknam, A.K. Fard, A. Seifi, Distribution feeder reconfiguration considering fuel cell/wind/photovoltaic power plants, Renew. Energy 37 (1) (2012) 213–225.
[37] G.D. Sen, J. Sharma, G.R. Goyal, A.K. Singh, A multi-objective PSO (MOPSO) algorithm for optimal active power dispatch with pollution control, Mathemat. Model. Eng. Probl. 4 (3) (2017) 113–119.
[38] S. Ke, J. Yang, L. Chen, P. Fan, X. Shi, J. Ligao, F. Wu, A Frequency Control Strategy for EV Stations based on MPC-VSG in Islanded Microgrids, IEEE Trans. Ind. Inf. (2023).
[39] P. Vidyasagar, K. Shanti Swarup, "LTI-MPC for the Micro-grid Control," *Design and Development of Model Predictive Primary Control of Micro Grids: Simulation Examples in MATLAB*, Springer, 2023, pp. 69–90.
[40] K. Feng, C. Liu, Adaptive DMPC-based frequency and voltage control for microgrid deploying a novel EV-based virtual energy router, IEEE Trans. Transp. Electrif. (2023).
[41] A.S. Omran, M.S. Hamad, M. Abdelgeliel, A.S. Abdel-Khalik, An adaptive model based on data-driven approach for FCS-MPC forming converter in microgrid, Int. J. Control Autom. Syst. 21 (11) (2023) 3777–3795.